Remote Sensing of Boundary Layer Temperature Profiles by a Scanning 5-mm Microwave Radiometer and RASS: Comparison Experiments

E. R. WESTWATER, Y. HAN, V. G. IRISOV, AND V. LEUSKIY

Cooperative Institute for Research in Environmental Sciences (CIRES), University of Colorado/NOAA Environmental Technology Laboratory, Boulder, Colorado

E. N. KADYGROV AND S. A. VIAZANKIN

Central Aerological Observatory, Microwave Remote Sensing Laboratory, Moscow, Russia

(Manuscript received 31 December 1997, in final form 15 July 1998)

ABSTRACT

Two techniques for deriving low-altitude temperature profiles were evaluated in an experiment conducted from November 1996 to January 1997 at the Boulder Atmospheric Observatory (BAO). The first used a scanning, single wavelength, 5-mm (60 GHz) microwave radiometer to measure vertical temperature profiles. Two radiometers were operated simultaneously; one used a discrete scan, the other scanned continuously. The second technique was a Radio Acoustic Sounding System (RASS) that operated at 915 MHz. Typically, radiometric profiles were produced every 15 min; those from RASS were 5-min segments taken every hour. Ground truth for the experiment was available from in situ measurements at the BAO. The BAO has an instrumented 300-m tower with 5-min measurements of temperature and relative humidity available at the surface and at altitudes of 10, 50, 100, 200, and 300 m. The tower measurements were occasionally supplemented with radiosonde releases and with hand-held meteorological measurements taken on the tower elevator.

The differences between the radiometers and the tower sensors were about 1°C rms. The accuracy using an in situ temperature measurement at the radiometer height as a predictor was also evaluated; at the 200- and 300-m levels, only about 4°C rms accuracies resulted. During the experiment, the RASS occasionally experienced radio frequency interference; to eliminate these effects, a quality-control algorithm for the RASS system was developed and evaluated. In addition, an experiment was held in September 1996 at the Department of Energy's Atmospheric Radiation Program Southern Great Plains site in north central Oklahoma. For this experiment, evaluations of a scanning 5-mm radiometer relative to 3-hourly radiosondes are presented. Quality control on the radiosondes was provided by comparisons with independent in situ surface and 60-m tower observations. The agreement between the radiometric profiles and the quality-controlled radiosondes was better than 1°C up to 800 m. Plans for future deployments of these instruments are discussed.

In addition to the in situ comparisons, theoretical analyses of the scanning radiometer systems were also conducted. The effects of angular resolution of the current system, noise level, prediction from in situ measurements, and vertical resolution were examined.

1. Introduction

Remote sensing of low-altitude temperature profiles is important for a variety of studies, including air pollution, air–sea interaction, and short-term meteorological forecasting. Two techniques show promise for routine unattended sensing of profiles during nonprecipitating conditions. The first uses a scanning, single wavelength, 5-mm (60 GHz) microwave radiometer to measure temperature and temperature gradient profiles (Troitsky et al. 1993; Westwater et al. 1998). These passive instruments are easily transportable and could be deployed, for example, in urban environments. We were able to deploy and evaluate two independent systems, one of which operated in a continuously scanning mode; the other operated at discrete angles. The development of these scanning radiometers is relatively new, and a thorough evaluation of their performance was desirable. A second technique was that of a Radio Acoustic Sounding System (RASS) that operates at 915 MHz (May et al. 1990). RASS is much more mature than the scanning radiometer technique and its deployment is widespread. RASS measures profiles of virtual temperature T_v, rather than kinetic temperature T. Typically, radiometric profiles are produced every 15 min, while those of RASS were 5-min segments taken every hour. Because of anticipated deployment of similar systems in an arctic environment, we were interested in evalu-

Corresponding author address: Dr. Ed Westwater, NOAA/ETL, M.S. R/E/ET1, 325 Broadway, Boulder, CO 80303-3328.
E-mail: ewestwater@etl.noaa.gov

ating and comparing these systems during winter conditions in Colorado, where large excursions in temperature are common. An earlier evaluation was based on data from a two-week experiment in September in Oklahoma (Westwater et al. 1998) and did not address the accuracy of the system during such winter conditions.

Obtaining accurate ground truth for such systems is not always simple because of the relatively high cost of radiosondes. Although we did use radiosondes in part of our evaluations, it was much more cost effective to take advantage of a 300-m meteorological tower that was operated by Environmental Technology Laboratory (ETL). Because of its high frequency of observations, every 5 min, an adequate volume of in situ comparisons was obtained over a large range of meteorological conditions. As our results will show, the performance of the radiometers was encouraging, and such instruments could be deployed for boundary layer monitoring.

2. Description of experiments

During November 1996–January 1997, we conducted an experiment to compare radiometers and RASS at the Boulder Atmospheric Observatory (BAO), near Erie, Colorado (Kaimal and Gaynor 1983). The BAO has an instrumented 300-m tower with 5-min measurements of temperature and relative humidity available at the surface and at altitudes of 10, 50, 100, 200, and 300 m above ground level (AGL). The tower measurements were occasionally supplemented with radiosonde releases and with hand-held meteorological measurements taken on the tower elevator. In addition to the elevator, the tower also has a carriage that is moveable from the bottom to the top of the tower. In the first month of the experiment, the discrete- and continuously scanning radiometers were operated at about the same altitude (10 m) AGL. To avoid possible radio interference between the local oscillators, one radiometer was suspended from the carriage on a boom at the 10-m level, while the other was located on a trailer about 25 m away. After a month of continuous and largely unattended operation, one radiometer was moved to the top of the tower, where it operated for another month.

ETL also participated in a second experiment that was conducted at the Department of Energy's Atmospheric Radiation Measurement (ARM) Program's Cloud and Radiation Testbed (CART) site in north central Oklahoma (Stokes and Schwartz 1994). This experiment was conducted during a two-week interval from 15 to 30 September 1996, during a water vapor intensive operating period (WVIOP'96) that was designed to study atmospheric water. Radiosondes were released every 3 h during the course of WVIOP'96, and temperature data from a 60-m meteorological tower were also available. During this experiment, the continuously scanning radiometer was deployed 3 m AGL on the top of a seatainer. The radiometer site was located 125 m from the radiosonde launch site and 101 m from the meteorological tower. Comparisons of radiometer temperature retrievals with measurements from the tower were reported by Westwater et al. (1998). Here, we present comparisons of the radiometer with radiosondes, using tower data as quality control on the radiosonde data. The quality control was frequently necessary, presumably because of radiosonde drift away from the tower and radiometer, and because of local inhomogeneity in the temperature field.

a. Description of radiometers

The discrete scanning radiometer was operated by the Central Aerological Observatory (CAO), Russia (Troitsky et al. 1993). The CAO radiometer was a commercially available instrument from the Russian firm ATTEX (Kadygrov and Pick 1998). The radiometer operated at a center frequency of 59.6 GHz, a 2-GHz bandwidth, and a 3-dB beamwidth of 6.0°. The manufacturer's specifications state a sensitivity of 0.04 K rms at 1-s integration time, a cycle time of 120 s for one profile measurement, a vertical resolution of 50 m, and an accuracy of 0.5 K rms up to 600 m. The continuously scanning radiometer operated by ETL (Trokhimovski et al. 1998; Westwater et al. 1998) had a receiver similar to that of ATTEX with a center frequency of 60.0 $\pm$ 0.1 GHz, a wider bandwidth (4 GHz), excellent sensitivity (0.03 K rms at 1 s), and its antenna was rotating at a rate of 1.3 Hz. The antenna was a corrugated conical horn with a 3-dB beamwidth of 7.5°. This radiometer was loaned to ETL by the Lebedev Physical Institute of the Russian Academy of Sciences, Moscow, Russia.

Data from both the ATTEX and the ETL radiometers were used to derive temperatures at the tower levels so that they could be compared directly with the in situ measurements. The ATTEX radiometric system had its own calibration reference that consisted of an in situ measurement of temperature at the height of the radiometer. This reference, therefore, constrained the brightness temperature measured when the radiometer pointed in the horizontal direction to be equal to the reference temperature. The ETL system did not have an associated in situ measurement; therefore, with the radiometer mounted at the 10-m tower level, we used the tower temperature measurement as the horizontal reference.

b. Estimation of vertical resolution

Although the ATTEX manufacturers specifications stated that the vertical resolution was 50 m from the surface to 600 m, we performed our own analysis of resolution. However, there are many subtleties concerned this concept as applied to radiometry or to inverse problems in general (Parker 1994). For example, the Rayleigh criterion (Born and Wolf 1964) associated with optics relates resolution to the wavelength sepa-

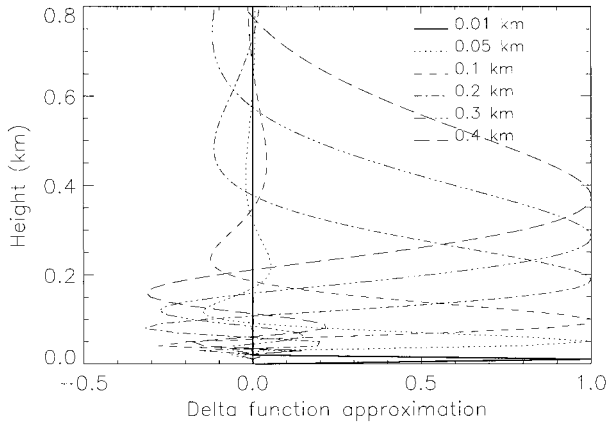

FIG. 1. Approximation to a Dirac delta function centered at the indicated heights constructed from a linear combination of temperature weighting functions for a scanning 5-mm radiometer. All functions are normalized to unit maximum.

ration by which two monochromatic components of equal spectral intensity can be resolved by an interferometer or spectrometer. Such a criterion could be applied to radiometric temperature retrieval, especially in linear problems, by defining suitable temperature excursions such that two excursion-thickness products could be resolved. However, such idealized temperature excursions would not be realized in nature. Parker (1994) suggests other measures, such as introducing a Dirac delta function [$\delta(h - h_0)$, where h = height] excursion at a point h_0 and then measuring the width of the retrieved profile. Other measures of resolution, suggested by Backus and Gilbert (1968), have been related to the degree to which linear combinations of the weighting functions [here, of the radiative transfer equation (RTE)] can be made to approximate a Dirac delta function, or the degree to which such linear combinations can minimize the so-called spread. Another consideration in the resolution question is how the existence of a priori information can influence the spread (Rodgers 1976). Here, we constructed the linear combination of temperature weighting functions $W_i(h)$ that minimized, in the least squares sense, the approximation to a delta function, that is, $\delta^*(h - h_0) \approx \delta(h - h_0)$, where

$$\delta^*(h - h_0) = \sum c_i(h_0)W_i(h), \tag{1}$$

$c_i(h_0)$ are the expansion coefficients, and we measured the resolution Δ as the full width, at half maximum, of $\delta^*(h - h_0)$. We constructed such a set of functions for a radiometer situated at 10 m AGL and for a pencil beamwidth. The so-constructed functions are shown in Fig. 1 and the resolution widths Δ are shown in Table 1. Thus we see that resolutions of about 65 m or better below 100 m are realized, and that the resolution degrades rapidly above this altitude. As a rough estimate of the resolution as a function of measurement height,

TABLE 1. Vertical resolution Δ (km) of scanning radiometer placed at 10 m AGL as a function of height h (m).

h	10	50	100	200	300	400
Δ	7.5	25	65	130	225	300

we found that $\Delta(h) = (h/h_0)\Delta(h_0)$. It is clear from the figure that only coarse information from the measurements themselves is available above 400 m. It is beyond the scope of this work to include a priori information in the estimate of resolution, although the statistical retrieval algorithm that we use on the ETL data does use this information.

c. Angular resolution of radiometers: T_b versus T_A

Another kind of resolution also affects the measurement accuracy, namely that of angular resolution of the antenna. As discussed by Ulaby et al. (1981), a radiometer measures the antenna temperature T_A, which is a weighted average over 4π steradians of the brightness temperatures T_b emitted by the atmosphere and the surface:

$$T_A(\theta_0, \varphi_0) = \frac{\iint T_b(\theta, \varphi)F_n(\theta, \varphi)\, d\Omega}{\iint F_n(\theta, \varphi)\, d\Omega}, \tag{2}$$

where

$T_A(\theta_0, \varphi_0)$ = antenna temperature at the observation angles θ_0, φ_0;
$T_b(\theta, \varphi)$ = brightness temperature at the angles (θ, φ) relative to the antenna coordinates;
$F_n(\theta, \varphi)$ = antenna power response function at (θ, φ);
(θ_0, θ) = polar angles;
(φ_0, φ) = azimuthal angles; and
$d\Omega = \sin(\theta)\, d\theta\, d\varphi$ = element of solid angle.

The power pattern $F_n(\theta, \varphi)$ for a corrugated conical horn antenna of the type used in our experiments, is a good approximation, independent of φ and of incident polarization, and was modeled, following Dragone (1977), as

$$F_n(\theta) = \left[u^2 \frac{J_0(v)}{u^2 - v^2}\right]^2, \tag{3}$$

where

$v = ka \sin\theta$, $0 \le \theta \le \pi/2$;
$F_n(\theta) = 0$, $\pi/2 \ge \theta \ge \pi$;
$k = 2\pi/\lambda$;
λ = wavelength;
a = diameter of conical horn;
J_0 = Bessel function of order 0; and
u = first zero of $J_0 = 2.4048$.

We first calculated the power pattern of our antenna using (3) with measured parameters a = 28.7 mm and λ = 5.0 mm. For these parameters, the 3-, 6-, and 10-dB beamwidths were 6.6°, 9.13°, and 11.44°; the width between the first nulls in the pattern was 17.59°; and the antenna directivity was 29.5 dB. We also compared our calculations of corrugated conical horn properties, based on (3), with more recent methods of determining the power pattern, as given by Pozar (1996), which yielded an estimate of the 3-dB beamwidth of 7.5° and directivity of 26.4 dB. In this case, we can still use (3) to calculate the antenna pattern if we replace the measured antenna radius, with an effective radius determined from the Pozar method. We used both measured and effective radii when calculating (2) and (3). We also compared our beamwidth calculations with those of Thomas (1978), who discussed various limiting cases of corrugated conical horn antennas.

Finally, to evaluate (2), we calculated both upward- and downward-flowing brightness temperatures from the RTE that assumes horizontal stratification, neglects refraction and earth curvature, and assumes specular reflection at the surface:

$$T_b^{\downarrow}(h_0, \theta) = \int_{h_0}^{\infty} T(h)\alpha(h) \exp\left[\frac{-\tau(h_0, h)}{\cos\theta}\right] \frac{dh}{\cos\theta}, \quad 0 \le \theta < \pi/2 \tag{4a}$$

$$T_b^{\uparrow}(h_0, \theta) = T_{b\text{sur}} + T_{b\text{refl}} + T_{b\text{emit}}, \tag{4b}$$

$$T_{b\text{sur}} = \epsilon T_S \exp\left[\frac{\tau(0, h_0)}{\cos\theta}\right], \quad \pi/2 < \theta \le \pi \tag{4c}$$

$$T_{b\text{refl}} = (1 - \epsilon) T_b^{\downarrow}(0, \theta) \exp\left[\frac{\tau(0, h_0)}{\cos\theta}\right], \quad \pi/2 < \theta \le \pi \tag{4d}$$

$$T_{b\text{emit}} = \int_0^{h_0} T(h)\alpha(h) \exp\left[\frac{\tau(h, h_0)}{\cos\theta}\right] \frac{dh}{\cos\theta}, \quad \pi/2 < \theta \le \pi \tag{4e}$$

and

$$\tau(h_1, h_2) = \int_{h_1}^{h_2} \alpha(h')\, dh'. \tag{4f}$$

In (4), we have $T_b^{\downarrow}(h_0, \theta)$ = downwelling brightness temperature at observation height h_0 and polar angle θ, and $T_b^{\uparrow}(h_0, \theta)$ = upwelling brightness temperature, ϵ = surface emissivity, T_s = surface skin temperature (K), $T(h)$ = temperature (K) at altitude h (km), $\alpha(h)$ = absorption coefficient (nepers km^{-1}), and $\tau(h_1, h_2)$ = optical depth between heights h_1 and h_2. In the limiting case when $\theta = \pi/2$ we have

$$T_b^{\downarrow}(h_0\ \pi/2) = T_b^{\uparrow}(h_0, \pi/2) = T(h_0). \tag{4g}$$

Finally, to transform coordinates from the cartesian system fixed to the antenna (θ, φ) with the system oriented at observation angles (θ_0, φ_0) to $T_b(\beta)$, we used

$$\cos(\beta) = \cos(\theta_0)\cos(\theta) - \sin(\theta_0)\sin(\theta)\cos(\varphi), \tag{5}$$

where β is the polar angle relative to the system in which the observation angles are measured and for which T_b is independent of the azimuth angle. Although we have developed computer software that integrates the RTE over a path that is refracted and curved by the earth, this complication is not necessary for calculating O_2 emission at 5 mm, where $\tau = 1$ at $h \approx 300$ m, and, hence, only paths less than or equal to about 1 km contribute to the emission. Both the calculations and the technique itself assume horizontal stratification over a distance of about a kilometer.

We carried out several numerical evaluations of (2) to (5) to determine, for the parameters of the scanning radiometer mounted at 10 m AGL, the degree to which T_A differs from T_b. We used the software package of Schroeder and Westwater (1991) together with the absorption algorithms of Liebe (1989) to calculate the emission. We calculated both downwelling and upwelling brightness temperatures for several radiosonde-measured profile types: two each of lapse, surface-based inversion, and elevated inversions, using Denver, Colorado, radiosonde data from the winter of 1996. We also chose three values of surface emissivity ϵ: ϵ = 0.55, 0.8, and 0.9, as well as three values of skin temperature: $T_S = T(0)$ (all types), $T(0) + 2$°C (lapse and elevated inversions) and $T(0) - 2$°C (surface-based and elevated inversions). The largest departure that we calculated was 0.30°C (for $0 \le \theta < \pi/2$) and both the T_b profile and the $T_b - T_A$ plots of this case are shown in Fig. 2. All of the calculated differences were with three standard deviations of the assumed noise levels that we used in temperature profile recovery (see section 2d). We note that for all profile types, the largest departures occurred when T_S differed the most from $T(0)$. In addition, the maximum departures of T_A and T_b were larger when the antenna was placed at h_0 = 3 m from those of h_0 = 10 m by about 0.2 K. We also found that only small differences (≤0.1 K) between T_A calculated with a 3-dB beamwidth of 6.6° and one with 7.5°. The effect of these differences on retrieved temperature profiles is discussed in section 3e.

d. Profile retrieval algorithms

Two profile retrieval algorithms were used to derive profiles from the 5-mm radiometer brightness temperature data. The first, used on the ATTEX radiometer data, was a variation of the Twomey–Tikonhov retrieval algorithm (Twomey 1977), and the details of this method, when applied to retrieval of temperature profiles from scanning radiometer data, are given by Troitsky et al. (1993) and Trokhimovski et al. (1998).

The second method, used on the ETL data, used a

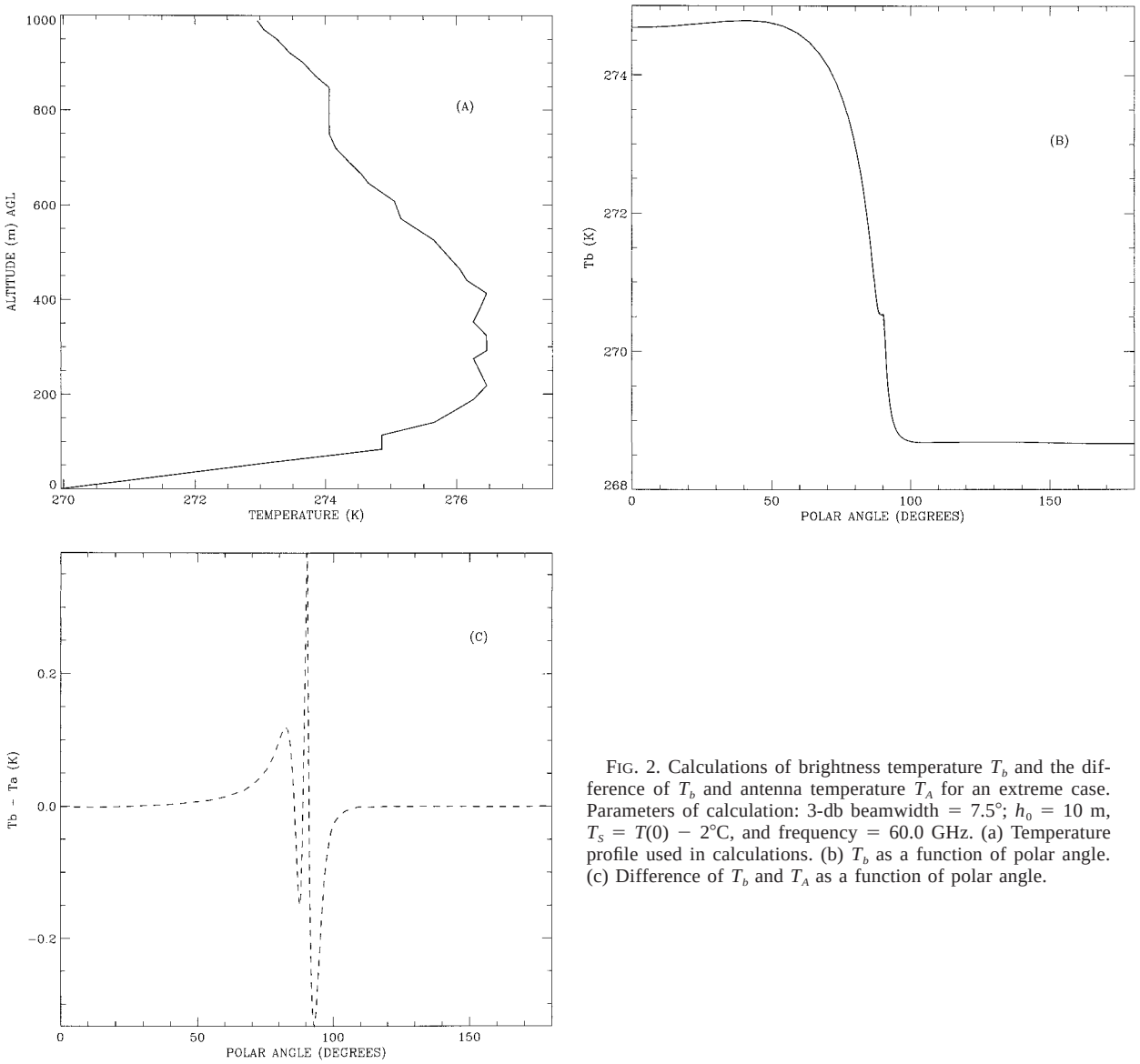

FIG. 2. Calculations of brightness temperature T_b and the difference of T_b and antenna temperature T_A for an extreme case. Parameters of calculation: 3-db beamwidth = 7.5°; h_0 = 10 m, $T_S = T(0) - 2$°C, and frequency = 60.0 GHz. (a) Temperature profile used in calculations. (b) T_b as a function of polar angle. (c) Difference of T_b and T_A as a function of polar angle.

variation of linear statistical retrieval (Westwater 1993) that derives lapse rate profiles from a projection of angular brightness temperature differences $\Delta T_b(\theta_i)$ on a set of empirical orthogonal functions. Here, $\Delta T_b(h_0, \theta_i) = T_b^{\downarrow}(h_0, \theta_i) - T_b^{\downarrow}(h_0, 0)$, where θ_i is the ith zenith angle, $i = 1, 2, \ldots, n$. More specifically,

$$(\mathbf{\Gamma}')^* = \langle \mathbf{\Gamma}' \mathbf{v}'^{\mathrm{T}} \rangle \langle \mathbf{v}' \mathbf{v}'^{\mathrm{T}} + \mathbf{S}_\epsilon \rangle^{-1}, \qquad (6)$$

where $(\mathbf{\Gamma}')^*$ = estimate of the departure of the lapse rate vector $\mathbf{\Gamma}$ from its ensemble average, $\mathbf{v}'$ = projection of the measurement vector $\Delta \mathbf{T}_b$ on first k empirical orthogonal vectors in brightness temperature space plus an additional component from the in situ temperature measurement at the height of the instrument, and $\mathbf{S}_\epsilon$ = $(k + 1) \times (k + 1)$ dimensional covariance matrix describing experimental errors. In (6), $\langle\ \rangle$ refers to ensemble averaging over a joint distribution of temperature and brightness temperature vectors, and the primes refer to departures from the ensemble means. To implement this algorithm, we constructed a 91 × 91 covariance matrix describing brightness temperature difference fluctuations at 90 equally spaced zenith angles ranging from 0 to $\pi/2$ plus in situ temperature, performed an eigenvector analysis on this covariance matrix evaluated, and, based on an assumed error level variance criteria of $\mathbf{S}_\epsilon = \mathrm{diag}(0.01K^2)$, used $k = 5$ for the retrieval analysis. The statistical database for the tower experiment was a 25-yr set of soundings (December–February) from Denver, Colorado; the a priori database for the Oklahoma experiment was a 4-yr set (August–November) from observations taken at the central CART site.

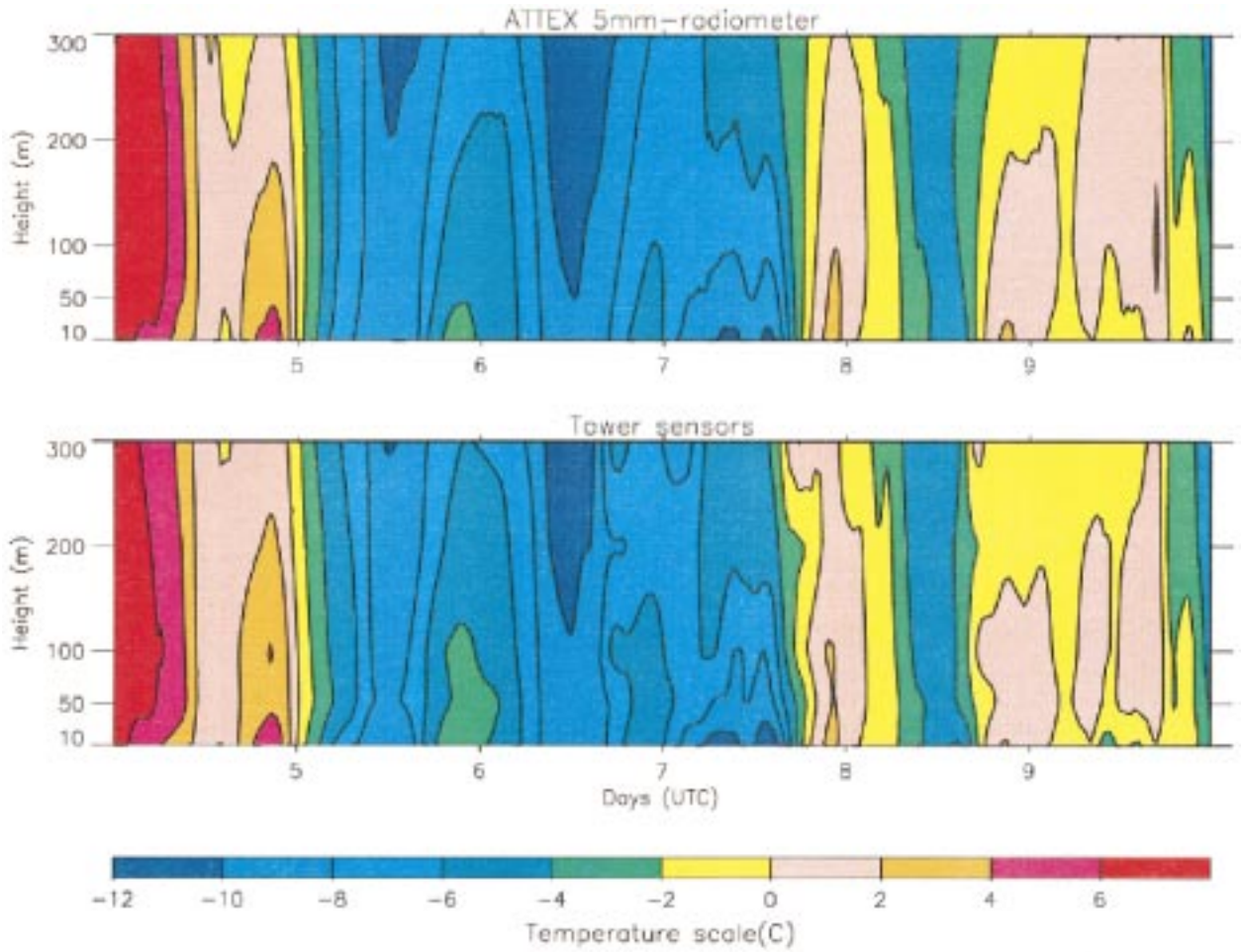

FIG. 3. Temperature time–height cross sections derived from ATTEX radiometer (top curve) and in situ sensors on BAO 300-m tower (bottom curve), 4–10 Jan 1997.

e. RASS at the BAO tower

The RASS system that we used was a commercial system purchased from Radian and has range gates centered at 135, 195 m, . . . , each with a vertical resolution and spacing of 60 m. For all practical purposes, the maximum range of this RASS system was 615 m. Because of reflections of the electromagnetic transmissions from metallic objects, RASS was located about 400 m away from the BAO tower. Virtual temperature soundings from RASS were obtained from 5-min data segments taken on the hour.

3. Results

a. Time–height cross sections

One of the advantages of the 5-mm radiometric data is continuity in time, which allows time series and time–height cross sections to be derived. We show examples in Figs. 3 and 4 of time–height cross sections taken during periods of substantial change in boundary layer temperature. From 4 to 5 January 1997, a cold air mass moved into the Rocky Mountain region, and the resulting surface temperature at the BAO changed from 7° to −9°C. The cold air reached a minimum temperature on 7 January, and then a sharp transition to a warm regime occurred about 1200 LT on that day. Warm temperatures then persisted for the next three days. Figure 3 shows a 10-day segment of data taken during these transitions between warm and cold conditions. The lower cross sections were obtained from BAO tower data (0–300 m) and the upper from the ATTEX radiometer (0–300 m); local time (MST) is used. We note a good qualitative agreement between the two datasets, each of which portrays the evolution of the atmospheric boundary layer. Figure 4 shows a 6-day cross section taken by the ETL radiometer during which there were again substantial changes in the temperature structure. As in the previous figure, the tower and radiometer data are in excellent agreement.

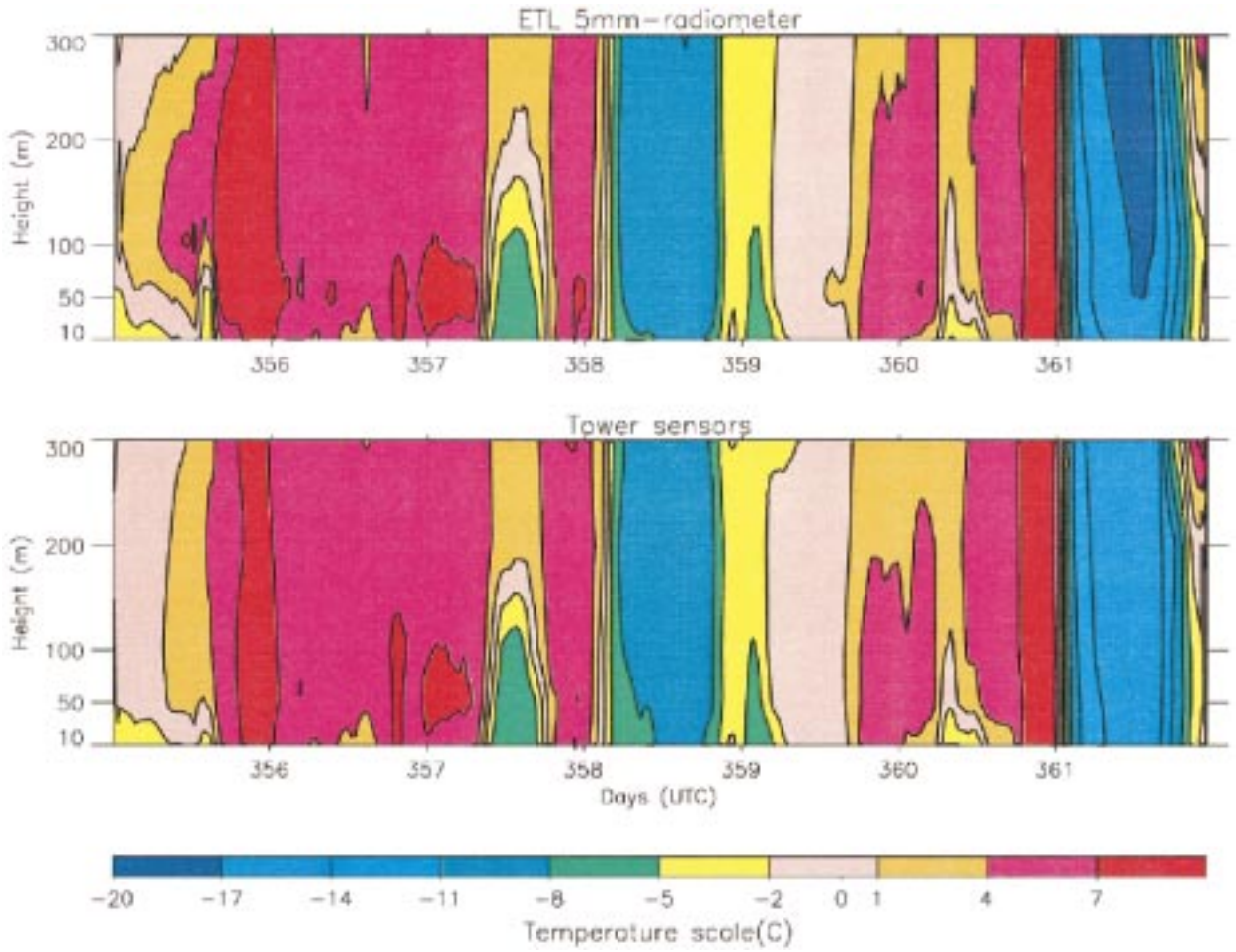

FIG. 4. Temperature time–height cross sections derived from ETL radiometer (top curve) and in situ sensors on BAO 300-m tower (bottom curve), 20–27 Dec 1996.

b. Time series

Figure 5 shows time series of temperature at the 200-m level for the two systems. In Fig. 5a, ATTEX, BAO, and RASS temperatures are shown. The 915-MHz RASS data were interpolated to tower levels for these comparisons. In preparing the RASS data for this figure, strict quality control methods (QC) were applied (see the following section). In addition, the RASS T_v values have been converted to T by use of the tower humidity measurements. From Fig. 5a, it is seen that all of the data follow each other closely, with the largest differences associated with the RASS system. Note the roughly 30°C ranges in temperatures during this 10-day time period and the rapid drop in temperature during 3 January. In Fig. 5b, we show a 6-day comparison of the ETL and the tower measurement. Again, over a 30°C range in temperatures and very sharp temporal changes in temperature, the radiometer and in situ sensor track each other to within about 2°C.

c. Quality-control method for RASS

The RASS data were available for us on the ETL Web site and formed a portion of the data base for a regional air pollution experiment also conducted by ETL. These data from the Web site had already been corrected for vertical wind velocities, and a consensus average QC had been applied to the data. However, even after the application of these methods, several large outliers remained. Discussions with an ETL scientist knowledgeable about RASS indicated that a recently installed commercial radio communications transmitter was giving radio frequency interference. Previous results (May et al. 1990) had yielded accuracy results of 0.5°C rms. In Fig. 6a, we show a scatterplot of RASS measurements, converted from T_v to T and interpolated to the 200-m tower level, versus the in situ measurements. It is obvious that without some additional QC, these data would be inadequate for most meteorological purposes. Since our radiometric comparisons with all of the tower levels were quite encouraging, we used the scanning radi-

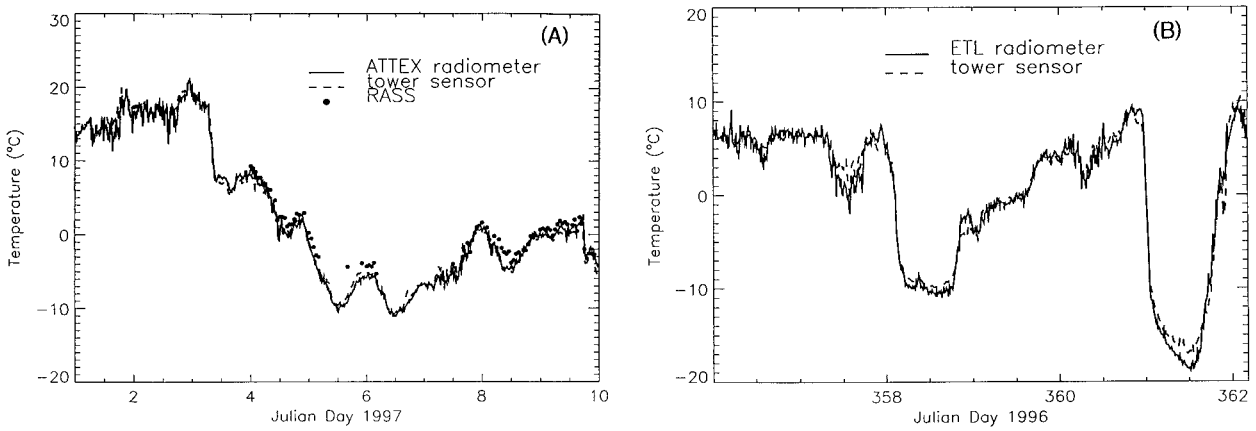

FIG. 5. (a) A 10-day time series of temperature at 200 m as measured by the ATTEX radiometer, by the in situ measurement on the tower, and by RASS, 1–10 Jan 1997. (b) A 6-day time series of temperature at 200 m as measured by the ETL radiometer and by the in situ measurement on the tower, 21–27 Dec 1996.

ometer to develop a QC method for RASS. Our method was quite straightforward: from the radiometer data, we had estimates, at each tower level, of the accuracy of the T retrieval; that is, the rms error σ and bias, as well as the regression line and its statistics. We also used surface humidity and pressure measurements to estimate T_v. If a RASS measurement, adjusted for bias, fell within a $\pm 3\sigma$ level of the estimated T_v, then the measurement was accepted; if not, the measurement was rejected. The scatterplot for the 200-m tower level, after QC is applied, is shown in Fig. 6b and a statistical summary is shown in Table 2. The improvement in every aspect is apparent.

d. Statistical comparisons with tower sensors

Comparison of tower and radiometer data indicated a potential problem with the tower temperature sensor at the 300-m level. Subsequently, it was found that a fan used to aspirate the temperature sensor had failed, and that during the day, solar heating was a problem. Thus, we eliminated from our statistical comparisons the daytime data at the 300-m level. In the first half of the experiment, the ETL radiometer was operated at the 10-m tower level; during the second half, the radiometer was elevated to the 300-m level and scanned the atmosphere above and below. Therefore, the sample size available for simultaneous comparisons of all upward-looking instruments was limited. In addition, the sample size of RASS data was reduced by about 25% due to QC criteria. Nevertheless, we think the available data were able to give at least a rough estimate of the accuracy of the systems. The statistical comparisons, shown in Table 3, indicate that the accuracy of ATTEX discrete scanning radiometer was always better than 1.0°C rms, and that of the ETL continuously scanning radiometer was slightly poorer by about 0.2°–0.3°C rms. These differences are statistically significant at the 99.5% level and could be due to a variety of causes, including different inversion methods or different data samples. Based on our experience with the ETL radiometer, we believe that the most probable cause of the

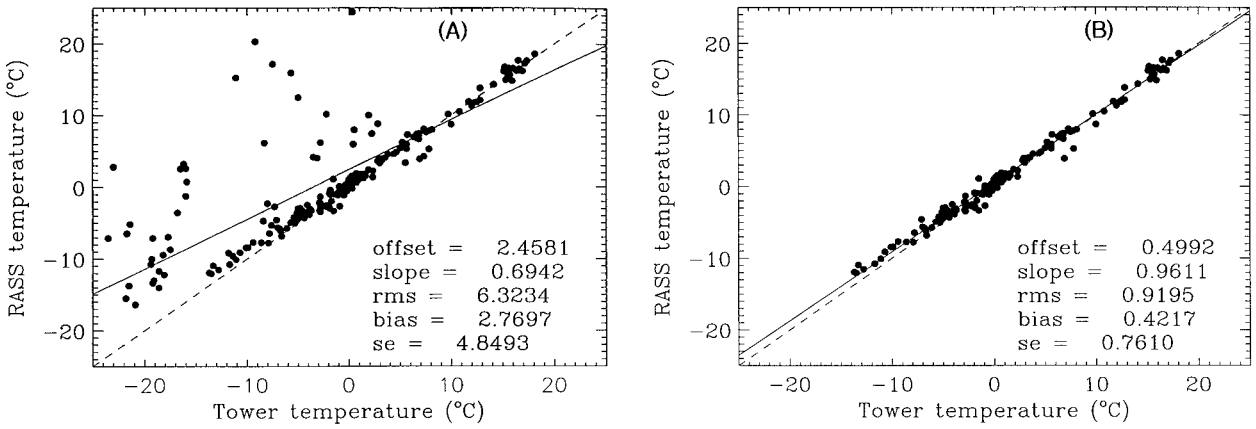

FIG. 6. (a) Scatterplot of RASS vs. BAO tower measurements at 200 m without quality control. Sample size = 215. (b) Scatterplot of RASS vs BAO tower measurements at 200 m using ATTEX radiometric temperature retrievals for quality control. Sample size = 166.

TABLE 2. Statistical comparisons between RASS and BAO tower measurements of temperature (°C).

Tower level	Before QC			After QC		
m	rms	bias	*n*	rms	bias	*n*
200	6.32	2.77	215	0.92	0.42	166
300	5.01	2.83	135	1.33	1.02	102

poorer performance is pointing drift of the rapidly scanning system. The next generation ETL radiometer will have a much better scanner/stepper motor to allievate this problem.

An anonymous reviewer stated that most of the accuracy achieved by the scanning radiometer was due to correlation of the temperature aloft with the in situ measurement at 10 m. To determine if this statement was true, we evaluated the accuracy to which the temperature could be predicted at each of the tower measurement levels using the 10-m in situ measurement as a predictor. We again used (1), but with υ being equal to $T_0 \equiv T(h = 10\text{ m})$. These results, together with the climatological variation over the period of the experiment, are also shown in Table 3. We note first, that although prediction with T_0 does reduce the variance, a residual standard deviation from 1.6° to 3.8°C remains. These results also show that a substantial additional reduction in standard deviation is achieved by the radiometric measurements (2.7 to 1 at 100 m and about 4 to 1 at the 200- and 300-m levels). In fact, even at the 50-m level, which is only 40 m above the reference level, a roughly 2 to 1 reduction in standard deviation is achieved. Thus, the reduction of the error to desirable levels (better than 1°C) was due completely to the scanning radiometer measurements.

Some insight why the residual error from using only T_s as a prediction is so large may be obtained from the scatterplots shown in Fig. 7. Figure 7a shows a scatterplot of tower temperature at 200 m versus the temperature predicted from T_0. It is seen that there are cluster of points in the lower diagonal half of the figure in which the slopes are nearly unity; that is, the predictions using T_0 are reasonably accurate. These, of course, come from lapse-type profiles in which there is good correlation between T_0 and the temperature aloft. However, in the upper-diagonal half, a significant number of points and clusters have no relationship at all with T_0. These points come from inversion-related profiles for which the correlation with T_0 is very low. None of the measures of fit, that is, slope, bias, offset, or rms difference, is really acceptable. As is seen in Fig. 7b, the additional information from the scanning radiometer almost completely removes the profile-type dependence from the results and yields almost no bias, a slope of nearly unity, an offset of nearly zero, and an rms difference of 0.81°C. Thus, the improved accuracy of the radiometric retrievals over that of T_0 predictions is due to the physical information content of the radiation measurements. In the arctic environment, where the radiometers will be deployed, winter conditions will be even less correlated with T_0.

e. Radiometric retrievals above 300 m: Comparisons with RASS

The top level of the BAO tower was 300 m, although both the 5-mm radiometers and RASS both gave measurements above this level. We realized that attenuation of the intervening atmosphere caused the radiometric retrievals to degrade with altitude. However, accuracy estimates of the radiometer at 400 and 500 m were around 1.0°C rms. To evaluate the accuracy of the radiometer at these levels, we simply compared the radiometric retrieval with RASS measurements that had been subject to quality control. In addition, to convert from T_v to T, we assumed that the mixing ratios at 400 and 500 m were equal to their measured values at 300 m. After screening for obvious outliers, we compared RASS and radiometric retrievals at the two upper levels and achieved rms differences of 0.87 and 1.07°C. The scatterplots of the comparisons are shown in Fig. 8. Note the diminished sample size from the 300-m comparisons; this is due to the limited availability of the RASS measurements at the 400- and 500-m levels.

f. Radiometric retrievals above 300 m: Comparisons with radiosondes

Data from WVIOP'96 were also available to evaluate retrieval accuracy above 300 m. However, only the ETL radiometer was operated during this experiment and both radiosonde and tower data were available for comparison. Previously, only data from the tower were eval-

TABLE 3. Statistical comparisons with BAO temperature measurements of temperatures derived from *T* (10 m), ATTEX radiometer, ETL radiometer, and RASS (°C).

Tower	Sample	*T* (10 m)			ETL			ATTEX			RASS		
level (m)	sde	rms	bias	*n*	rms	bias	*n*	rms	bias	*n*	rms	bias	*n*
10	10.7	—	—	—	—	—	—	0.9	0.3	2103	—	—	—
50	11.2	1.7	−0.2	2103	1.0	0.0	2351	0.9	−0.3	2103	—	—	—
100	11.4	2.3	0.3	2103	1.2	−0.6	2351	0.9	−0.1	2103	—	—	—
200	11.5	3.6	−1.1	2103	1.0	−0.4	2351	0.8	−0.1	2103	0.9	0.4	166
300	11.2	3.8	1.1	1243	1.2	0.0	1403	0.9	0.2	1243	1.3	1.0	104

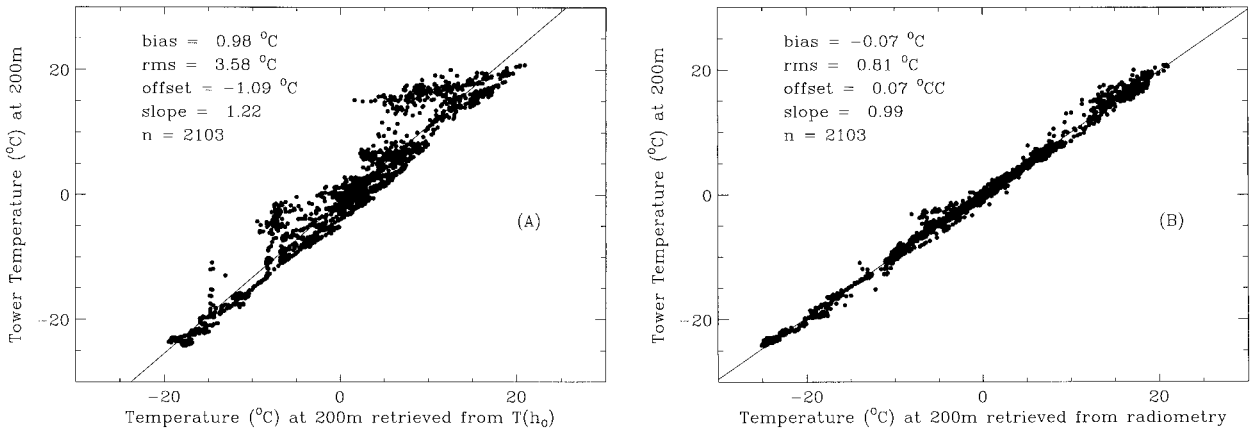

FIG. 7. Scatterplot of temperature retrievals vs tower measurements at 200 m. (A) Temperature retrieved from in situ measurement at 10 m. (B) Temperature retrieved from ATTEX scanning radiometer measurements.

uated by Westwater et al. (1998). It was found, by comparisons of radiometer, radiosonde, and tower data, that substantial differences between the sensors sometimes occurred. It was likely that these differences were the result of spatial inhomogeneity in the boundary layer. Here, since we wanted to achieve a realistic estimate of the accuracy of temperature retrieval, especially above 300 m, we used the tower data (at 25 and 60 m) to quality control the radiosonde data. If the radiosonde differed from the tower by greater than 1.5°C, we did not use the data.

One other feature of our data requires mention. Because the terrain differed modestly from one side of the scan to the other, we had noticed previously (Westwater et al. 1998) that east and west scans were sometimes different. For the present analysis, we separated our retrievals into east and west scans for comparison with radiosondes. Typical profile retrievals are shown in Figs. 9a,f. We note in these cases that the radiometric retrievals agree with the radiosonde up to within 1°C below 400 m; however, as seen in Figs. 9e,f, elevated inversions above 500 m are very difficult to resolve with this passive technique. Similar conclusions were reached by Miller and Falls (1989).

From the retrievals, we computed error statistics as a function of altitude. However, it is also of interest to determine theoretically what this performance should be, especially as a function of radiometer noise levels σ_ϵ. From the same a priori database that we used to derive retrieval coefficients, we estimated retrieval accuracy as a function of radiometer accuracy. These results are shown in Fig. 10a, for σ_ϵ ranging from 0.01 to 0.5 K rms. We also wanted to evaluate the hypothesis advanced by the anonymous reviewer that most of the predictive ability of the scanning system came mostly from the surface measurement. Even though the a priori climatology is that of Oklahoma during August–November, and might be to expected to be better predicted from $T(h_0)$ than that of Denver, again the predictive ability is worse than 3°C rms above 100 m AGL and falls to about 4.5°C rms above 500 m AGL. For the predicted radiometric errors, we note that only a small

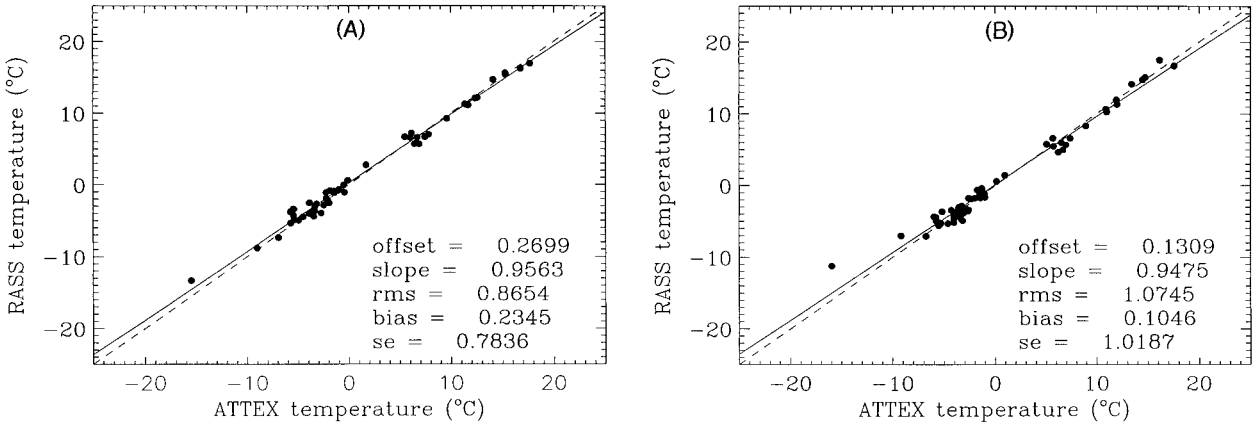

FIG. 8. Scatterplot of ATTEX radiometer vs RASS temperature measurements. RASS T_v measurements have been converted to T by use of tower humidity measurements at the 300-m level. (a) 400 m, sample size = 58. (b) 500 m, sample size = 58.

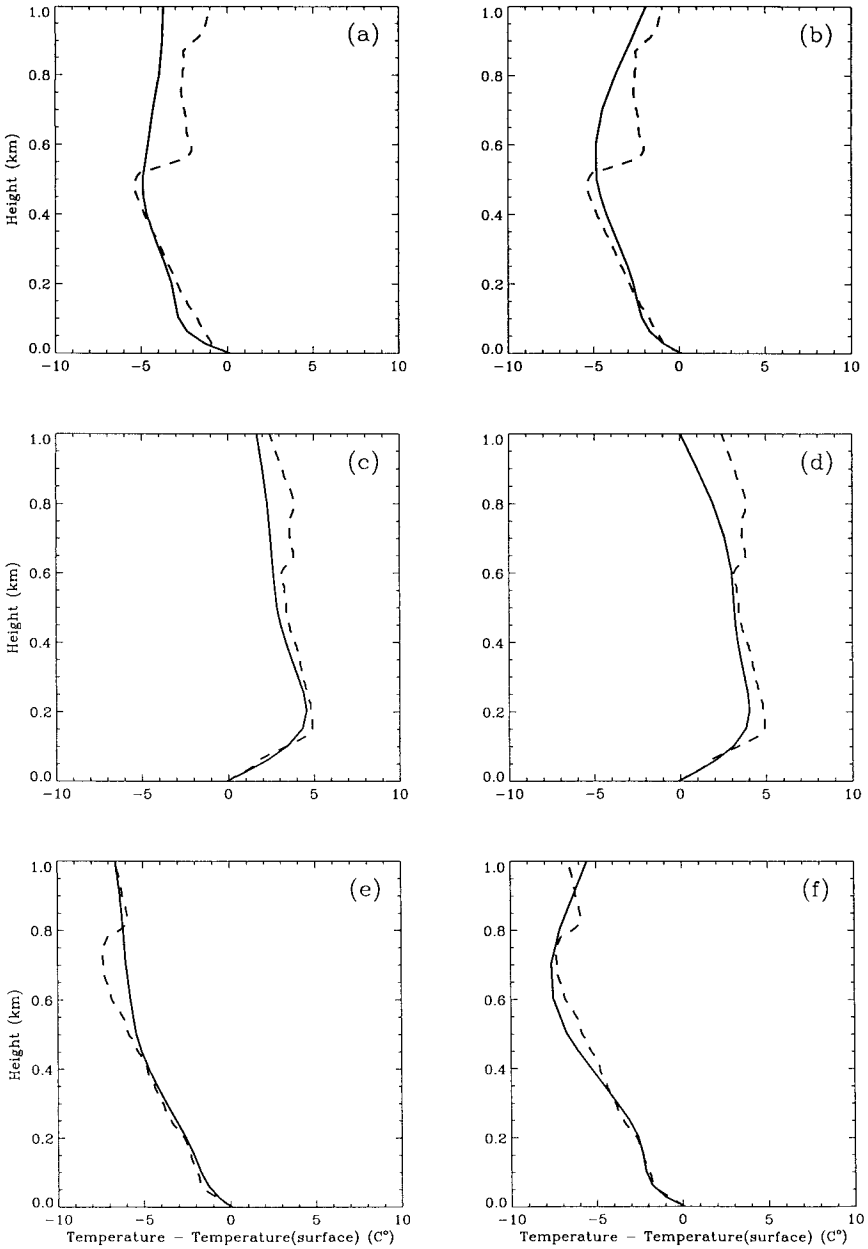

FIG. 9. Profiles of temperature as measured by the ETL scanning radiometer (solid curves) and by radiosondes (dashed curves) at the ARM SGP CART site. Figures (a), (c), and (e) are from the east scan, while (b), (d), and (f) are from the west scan. (a) and (b) are from 1730 UTC 12 Sep 1996; (c) and (d) are from 0828 UTC 26 Sep 1996, and (e) and (f) are from 1440 UTC 12 Sep 1996.

difference in retrieval error is predicted for σ_ϵ between 0.01 and 0.1 K rms. However, a substantial difference is predicted between the 0.1 and 0.5 K levels, especially below 400 m. We believe that our system noise level is close to the 0.1 K level. However, as was shown in section 2c, that if the skin and air temperatures differed by 2 K, the difference between T_b and T_A could be as large as 0.3 K. Referring to Fig. 10a, the difference between a 0.1 K and a 0.3 K error could be as large as 0.2 K, at least in the rms sense. The achieved retrieval difference statistics as a function of altitude are shown in Fig. 10b. As expected, the achieved results are somewhat larger than theoretical predictions (say for the 0.1 noise level) since, of course, the radiosonde has its own errors, and spatial and temporal differences also enter into the difference statistics. It could be, however, that we underestimated our effective system noise level, and that 0.5°C rms may be appropriate. We also note that

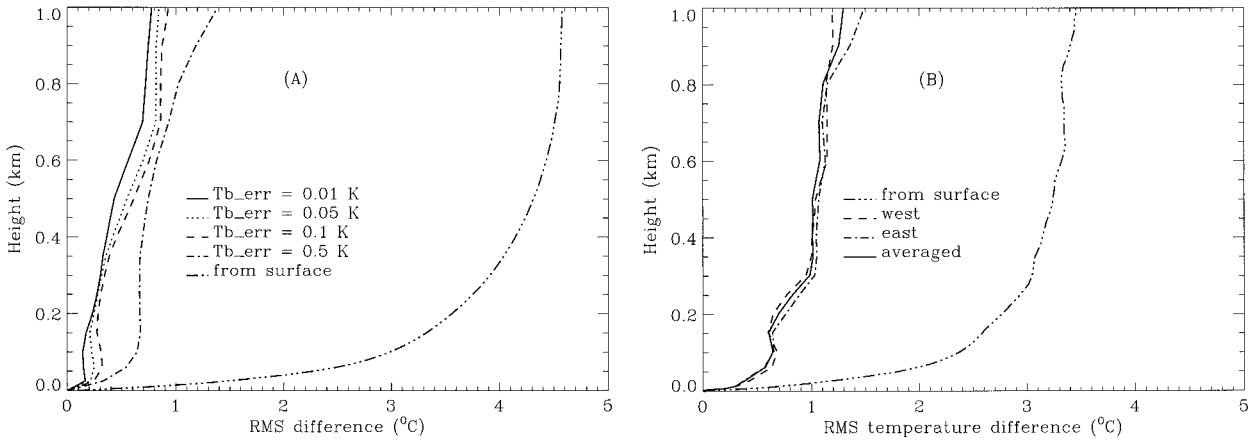

FIG. 10. (a) Theoretical accuracy of 5-mm scanning radiometer as a function of height for various choices of radiometer error and for prediction based on surface observations. (b) Rms differences as a function of height above the surface between profiles of temperature as measured by the ETL scanning radiometer, as estimated by surface temperature, and measured by radiosondes at the ARM SGP CART site.

the achieved error statistics are consistent with those obtained at the BAO tower (see Figs. 7 and 8 and Table 4).

g. Combined radiometric RASS retrievals

The prospects for combining RASS and radiometric retrievals from the scanning radiometer are intriguing. The ability of the radiometer to measure temperature from the surface to 300 or 400 m, the region of overlap between radiometer and RASS, and the potential of RASS to probe much higher than the radiometer, all suggest that such a combination would be fruitful. In Fig. 11, we show temperature profiles from the radiometer, RASS, and the tower. There is a region of overlap where the retrievals agree well with other, as well as nonintersecting regions, where each system could independently contribute information. A variety of retrieval algorithms could be used to combine such data if the accuracies of the data; that is, their error covariance matrices are known (Westwater 1993).

As another measure of how well a RASS could supply additional information to the radiometer, we determined the relative hourly sample sizes, before quality control, which were produced by RASS. May et al. (1990) have discussed how a 915-MHz RASS is subject to an appreciable amount of acoustic attenuation that limits its upper-altitude coverage. For the system deployed by ETL during this experiment, the relative frequency of data availability is given in Table 4. Relative sample sizes were roughly cut in half for each consecutive range gate above 495 m.

TABLE 4. Relative sample size N achieved by RASS during BAO experiment as a function of height h (m).

h (m)	135	195	255	315	375	435	495
N	250	268	251	204	187	131	92

4. Concluding remarks

Scanning radiometers at 5-mm wavelengths, both of ATTEX and of ETL, gave excellent comparisons with in situ temperature measurements during winter conditions at the BAO 300-m tower; several days of data were obtained during a snow storm, with no degradation of the quality of the data. A limited number of comparisons with the 915-MHz RASS above tower levels showed the ability of the radiometer to derive temperature profiles to about 500 m with an accuracy of about 1.0°C rms. During these experiments, the RASS system was subject to severe radio frequency interference; to eliminate spurious data, a quality-control method, based on radiometric temperature soundings, was developed and successfully applied to the data. About 75% of the RASS data passed the QC criterion and yielded accuracies, relative to tower measurements, of better than 1.3°C rms.

At the suggestion of an anonymous reviewer, we compared our temperature retrievals with those estimated

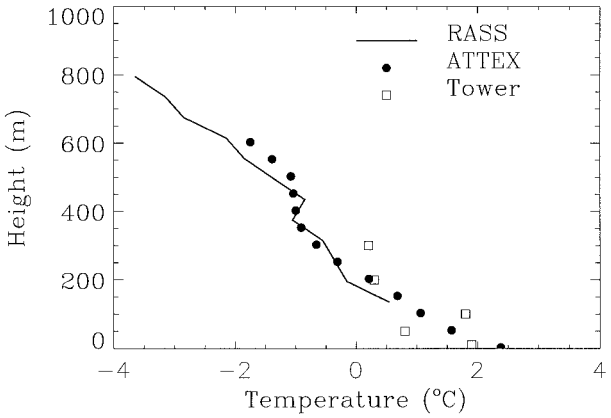

FIG. 11. Profiles of temperature as measured by the ATTEX radiometer, RASS, and BAO in situ sensors, 2100 UTC 7 Jan 1997.

from the temperature at measurement height. For the winter climatology that existed during the BAO experiments, only a 2° to 4°C rms accuracy was achieved above 100 m using the surface measurements, and the addition of the radiometer measurements reduced the residual rms difference to about 0.9°C rms.

To determine accuracy above the 300-m level, we also compared radiometric temperature soundings with those from radiosondes, using data from a 15-day experiment at the ARM CART site in north central Oklahoma. Below 300 m, these results also were consistent with those from the tower experiment and above, rms accuracies of less than 1.0°C up to 800 m AGL were achieved. However, it was apparent that elevated inversions above 500 m would be difficult to retrieve with this technique. We also investigated the accuracy in using surface temperature as a predictor and the improvement in accuracy that is achieved by using the scanning radiometer measurements. Here, as in the Colorado experiments, a reduction of standard deviation from 3° to 4°C rms was realized.

We supplemented the in situ data comparisons with supporting theoretical analyzes. First, the vertical resolution of the system was evaluated, and resolutions from 7 to 300 m were estimated, using as our measure of resolution the widths of functions that were constructed to approximate a Dirac delta function. We plan to evaluate the improvement of resolution that the introduction of a priori statistics can achieve. Next, we evaluated the effect of the finite beamwidth of our system (3-dB beamwidth of 7.5° for a corrugated conical horn antenna) and estimated that differences between antenna and brightness temperatures of 0.3°C could exist at near horizontal viewing. The largest factor in the brightness difference was the difference between air and skin temperature at the surface. We also evaluated for the Oklahoma August–November climatology and for a number of assumed radiometer noise levels, the predicted accuracy of the temperature profile retrievals. For the rms level that we used in our retrieval algorithm, 0.1 K rms, accuracies of better than 1.0°C could be achieved up to 1 km. However, the results that we obtained were more consistent with an effective noise level of 0.5 K rms. An effective noise level might include the effects of a nonstratified atmosphere and skin temperatures that depart considerably from local air temperatures. For example, we found that when the skin temperature differed by 2 K from the air temperature, T_A could differ from T_b for angles within 2° of horizontal. We did not have skin temperature measurements during either of our experiments, but a difference of 2 K, especially during the Oklahoma experiments would not be unreasonable. However, the representativeness of radiosondes in determining boundary layer temperatures on this scale could also contribute to the measured differences. If we assume two optical depths ($\tau = 300$ m for the 5-mm radiometer) as a representative horizontal scale, then significant horizontal temperature variations over this distance could cause error. However, the scanning radiometer, in its present configuration, allows opposite scans, as well as their average, to be examined. Our experimental results, as shown in Fig. 10b, yielded differences of less than about 0.1°C rms up to 800 m for the different scan combinations. Thus, except under extreme conditions of surfaces with substantially different heat fluxes surrounding the radiometer, departures from stratification do not seem to be a major problem.

As mentioned above, during cases in which the skin temperature differs appreciably from the air temperature, some measurement errors will occur for elevation angles less than about 2°. Several possibilities could reduce this error. One technique would be to use deconvolution to estimate lower angle T_b's. Another, would be to use a near ambient blackbody target for a calibration source, and eliminate the need for a horizontal reference.

We are constructing a scanning infrared radiometer that will be used in tandem with the scanning 5-mm radiometer, primarily for sea–air interaction studies. However, over a land surface, the scanning radiometer could also provide valuable information on skin temperature, and the two instruments together could provide information on microwave emissivity, as well.

As a part of the U.S. Department of Energy's Atmospheric Radiation Program (ARM), an ATTEX radiometer was purchased and will be deployed in their new facility on the North Slope of Alaska (NSA); an ETL 5-mm radiometer will be deployed there as well during an experiment to be condicted in the spring of 1999. To derive profiles above 300 m, ARM will deploy a RASS system at 915 MHz. We believe that the quality-control method that we derived here would be applicable to RASS, and that RASS and radiometers could make a useful combined remote sensing system.

Acknowledgments. This study was partially supported by the Environmental Sciences Division of the Department of Energy as a part of their Atmospheric Radiation Measurements Program. The authors thank J. B. Snider and J. R. Jordan for useful comments on the manuscript. The authors also acknowledge the comments of anonymous reviewers in improving and clarifying certain portions of the manuscript.

REFERENCES

Backus, G. E., and F. Gilbert, 1968: The resolving power of gross earth data. *Geophys. J. Roy. Astron. Soc.*, **16,** 169–205.

Born, M., and E. Wolf, 1964: *Principles of Optics.* The McMillan Company, 808 pp.

Dragome, C., 1977: Characteristics of a broadband microwave corrugated norm—A comparison between theory and experiment. *Bell Syst. Tech. J.*, **56,** 869–888.

Kadygrov, E. N., and D. R. Pick, 1998: The potential for temperature retrieval from an angular-scanning single-channel microwave radiometer and some comparisons with in situ observations. *Meteor. Appl.*, **5,** 393–404.

Kaimal, J. C., and J. E. Gaynor, 1983: The Boulder Atmospheric Observatory. *J. Climate Appl. Meteor.*, **22,** 863–880.

Liebe, H. J., 1989: MPM—An atmospheric millimeter wave propagation model. *Int. J. Infrared Millimeter Waves,* **10,** 631–650.

May, P. T., R. G. Strauch, K. P. Moran, and W. L. Ecklund, 1990: Temperature sounding by RASS with wind profiling radars. *IEEE Trans. Geosci. Remote Sens.,* **28,** 19–28.

Miller, P. A., and M. J. Falls, 1989: Pilot study of methods to decrease measurement errors of tropospheric inversions by ground-based microwave radiometry. *J. Atmos. Oceanic Technol.,* **6,** 225–234.

Parker, R. L., 1994: *Geophysical Inverse Theory.* Princeton University Press, 386 pp.

Pozar, D. M., 1996: PCAAD 3.0: Personal computer Aided Antenna Design. Antenna Design Associates, Leverett, MA, 59 pp. [Available from David M. Pozar, Antenna Design Associates, Inc., 55 Teawaddle Hill Rd., Leverett, MA 01002.]

Rodgers, C. D., 1976: The vertical resolution of remotely sounded temperature profiles with a priori statistics. *J. Atmos. Sci.,* **33,** 707–709.

Schroeder, J. A., and E. R. Westwater, 1991: Users' Guide to WPL Microwave Radiative Transfer Software. NOAA Tech. Memo. ERL-WPL 213, 84 pp.

Stokes, G. M., and S. E. Schwartz, 1994: The Atmospheric Radiation Measurement (ARM) Program: Programmatic background and design of the cloud and radiation test bed. *Bull. Amer. Meteor. Soc.,* **75,** 1201–1221.

Thomas, B. M., 1978: Design of corrugated conical horns. *IEEE Trans. Antennas Propag.,* **AP-26,** 367–372.

Troitsky, A. V., K. P. Gaikovich, V. D. Gromov, E. N. Kadygrov, and A. S. Kosov, 1993: Thermal sounding of the atmospheric boundary layer in the oxygen band center at 60 GHz. *IEEE Trans. Geosci. Remote Sens.,* **31,** 116–120.

Trokhimovski, Yu. G., E. R. Westwater, Y. Han, and V. Ye. Leuskiy, 1998: Air and Sea Surface Temperature Measurements Using a 60 GHz Microwave Rotating Radiometer. *IEEE Trans. Geosci. Remote Sens.,* **36,** 3–15.

Twomey, S., 1977: *Introduction to the Mathematics of Inversion in Remote Sensing and Indirect Measurements.* Elsevier, 243 pp.

Ulaby, F. T., R. K. Moore, and A. K. Fung, 1981: *Microwave Remote Sensing, Active and Passive.* Vol. I, *Microwave Remote Sensing Fundamentals and Radiometry,* Addison-Wesley, 456 pp.

Westwater, E. R., 1993: Ground-based microwave remote sensing of meteorological variables. *Atmospheric Remote Sensing by Microwave Radiometry,* M. A. Janssen, Ed., J. Wiley and Sons, Inc., 145–213.

——, Y. Han, V. G. Irisov, V. Ye. Leuskiy, Yu. G. Trokhimovski, C. W. Fairall, and A. T. Jessup, 1998: Air–sea and boundary-layer temperatures measured by a scanning 60-GHz radiometer: Recent results. *Radio Sci.,* **33,** 291–302.